Electronic Supplementary Material (ESI) for Dalton Transactions.
This journal is © The Royal Society of Chemistry 2022

Supporting Information

Efficiently increasing low-field magnetic entropy by incorporating SO_3^{2-} into $Gd_{22}Ni_{21}$ cluster

Ning-Fang Li, Ye-Min Han, Jia-Nian Li, Qiaoling Chen and Yan Xu*[,†,§]

[†] *College of Chemical Engineering, State Key Laboratory of Materials-Oriented Chemical Engineering, Nanjing Tech University, Nanjing 210009, P. R. China.*
[§] *State Key Laboratory of Coordination Chemistry, School of Chemistry and Chemical Engineering, Nanjing University, Nanjing 210023, P. R. China.*
E-mail: yanxu@njtech.edu.cn

Content

Section 1. Experimental Section

Materials and Physical measurements

All materials, reagents and solvents were of commercial origin and were used as received. Elemental analyses (C, H, N, S) were performed on a Perkin-Elmer 2400 elemental analyzer. Powder X-ray diffraction (PXRD) was recorded on a Bruker D8X diffractometer equipped with monochromatized Cu-K$_\alpha$ (λ = 1.5418 Å) radiation at room temperature. Data were collected in the range of 3-50°. Infrared spectra (FT-IR) of compounds were recorded with a Nicolet Impact 410 FTIR spectrometer with pressed KBr pellets, from 4000 to 400 cm^{-1}. Thermogravimetric analysis (TGA) measurement was carried out with a NETZSCH STA409 thermogravimetric analyzer in a flowing nitrogen atmosphere from 25 to 1000 °C with a heating rate of 10 K·min^{-1}. Energy dispersive spectrometer (EDS) were determined by using a Hitachi S-4800 scanning electron microscope at an accelerating voltage of 20 kV. The direct current magnetic data were measured at temperature between 1.8 and 300 K, and the magnetization isothermal measurements were made in fields of between 0 and 7 T on MPMS-XL7 SQUID magnetometer. Experimental susceptibilities were corrected for the diamagnetism estimated Pascal's tables and for sample holder by previous calibration. Gas chromatographic (GC) analysis was conducted by gas chromatography (FULI-9790II) with Thermal Conductivity Detector (TCD) and a Parapak-Q column (2 m × 3 mm). Experimental conditions were as follows: N_2 (99.99%) as Carrier gas; column temperature: 60 °C; injector temperature: 80 °C; Detector temperature: 90 °C; carbon dioxide (99.9 %) and air as quantitive analysis standard.

X-ray Crystallographic Study

The single crystal X-ray diffraction of the compound was tested through a Bruker Apex II CCD by using ω-2θ scan method with Mo-K$_\alpha$ radiation (λ =0.71073

Å). The crystalline structures were settled by direct method and refined by the fullmatrix least-squares methods on F^2 using the SHELX-2018/3 program package for compound **$Gd_{22}Ni_{21}$**. The free refinement gives the occupancy factor of Gd5 is 0.3739, which fixed 1/3 in the final refinement. While SO_4^{2-} and SO_3^{2-} groups are also disordered, the occupancy factors are 0.5 (for S1A and S2) and 0.25 (for S1B). The crystallographic data are presented in CIF files.

Table S1 The Crystallographic data of compound **$Gd_{22}Ni_{21}$**.

Compound	**$Gd_{22}Ni_{21}$**
Empirical formula	$C_{108}H_{202.75}Cl_{9.75}Gd_{22}N_{21}Ni_{21}O_{198.5}S_{3.75}$
Formula weight	10129.92
Temperature (K)	296(2)
Wavelength (Å)	0.71073
Crystal system	Hexagonal
Space group	*P*-6(2)*/c*
a (Å)	21.5001(12)
b (Å)	21.5001(12)
c (Å)	34.195(3)
α (°)	90
β (°)	90
γ (°)	120
Volume (Å^3)	13689.1(19)
Z	2
Calculated density (Mg / m^3)	2.458
Absorption coefficient (mm^{-1})	6.887
F(000)	9615
Crystal size (mm^3)	0.130 × 0.120 × 0.120
Limiting indices	-25<=*h*<=25, -25<=*k*<=25, -40<=*l*<=40
Reflections collected	97131
Independent reflection	8208 [*R*(int) = 0.0829]
Theta range for data collection (°)	1.245 to 25.022
Data / restraints / parameters	8208 / 289 / 668
Goodness-of-fit on F^2	1.038
Final *R* indices [I > 2sigma(I)][ab]	R_1 = 0.0309, wR_2 = 0.0772
R indices (all data)	R_1 = 0.0372, wR_2 = 0.0805
CCDC	2018460

[a]$R_1 = \Sigma||F_o|-|F_c||/\Sigma|F_o|$, [b]w$R_2 = \Sigma[w(F_o^2-F_c^2)^2]/\Sigma[w(F_o^2)^2]^{1/2}$

Section 2. Synthesis and Discussion

Synthesis of compound $Gd_{22}Ni_{21}$

$Gd(NO_3)_3·6H_2O$ (0.18 g, 0.40 mmol), $Ni(CH_3COO)_2·4H_2O$ (0.12 g, 0.50 mmol), iminodiacetic acid (H_2IDA; 0.06 g, 0.5 mmol), and imidazole (0.07 g, 1.00 mmol), were dissolved in the mixed solvent of CH_3CH_2OH/H_2O (v/v = 10 mL : 4 mL). This solution was stirred for 2 h under the room temperature, then Na_2SO_3 (0.01 g, 0.09 mmol) was added to the mixture and continued to be stirred another 10 minutes. Whereafter, the pH value of the solution was adjusted to about 3.0 (HCl, 1 M). Finally, this mixture was sealed in a 25 mL Teflon-lined autoclave and heated at 180 °C for 8 days before cooled down to the room temperature. Grass green diamond crystal **$Gd_{22}Ni_{21}$** was collected and dried in air (yield: 21.00 % basis on Gd). Elemental analysis: calculated (%): C, 12.80; H, 2.00; N, 2.90; S, 1.20; found (%): C, 12.75; H, 1.97; N, 2.90; S, 1.38.

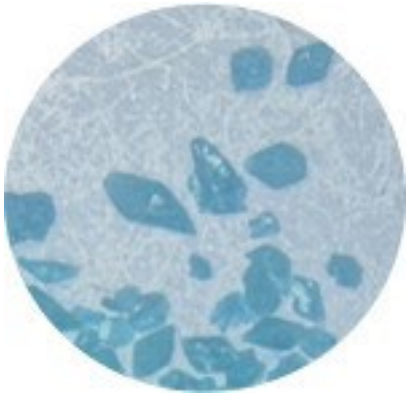

Fig. S1 The crystal morphology of **$Gd_{22}Ni_{21}$**.

Synthetic discussion

We had a desperate moment to synthesize new sulfite-doped 3d-4f high-nuclearity clusters. Various experimental attempts were conducted in the original period, but unfortunately, they all failed. Some synthetic factors must be fully considered during the synthesis, which are of great importance for the formation

of compound **$Gd_{22}Ni_{21}$**. Although imidazole was used as one of the initial reactants, we noticed that no imidazole was found in the final structures. However, we cannot obtain the target product without the addition of imidazole. In addition, imidazole plays an important role in stabilizing the structure of the cluster. Other bases (such as NaOH, triethylamine, 2-nitroimidazole, 1-benzylimidazole, 1,2,4-triazole, *etc.*) cannot complete the construction of this huge molecule. The pH value for the crystal growth is in the range of 2.5-3.5, however, the optimal value is 3.0. No crystalline products were obtained when the pH value was adjusted to lower than 2.5 or higher than 3.5. **$Gd_{22}Ni_{21}$** can be synthesized under the temperature 180 °C. In addition to the given synthesis temperature, no products were found at other temperatures. In this work, the Cl^- ions acted as the counter anions and come from the pH-adjusting (HCl). When HCl was changed into HNO_3 or HBr, there were on objectives. No products were obtained by directly adding NH_2CH_2COOH or $HOCH_2COOH$, which implied that slowly releasing or production small species ($HOCH_2COO^-$) played pivotal influence on the successfully assembly of these aggregations.

Among the methods for slowly introduction of CO_3^{2-}, atmospheric CO_2 fixation and the decomposition of some organic ligands have been widely accepted.[1] In this work, slowly rntroduction of CO_3^{2-} plays the the crucial influence on the successfully assembly of this aggregation, because no objective products were obtained by adding carbonate (Na_2CO_3, K_2CO_3, $NaHCO_3$, or $KHCO_3$). Meanwhile, CO_3^{2-} ions exist in **$Gd_{22}Ni_{21}$** with the following reasons: (i) FT-IR shows that the peak at 1445 cm^{-1} is attributed to C=O stretching and bending vibrations, indicating the presence of CO_3^{2-}; (ii) In order to further confirm the presence of CO_3^{2-} groups, compound **$Gd_{22}Ni_{21}$** (30 mg) was put in a 2 mL glass vial containing 1.2 mL H_2O. The mixture was stirred for 10 min under room temperature. And then 0.2 mL gas from this glass is collected with a sealing needle and injected into a gas chromatograph for analysis (Fig. S4a, S5). Later, a few bubbles appeared after injecting concentrated H_2SO_4 (80 μL, 18.4 mol/L). This can be ascribed to the destruction of the structure of compound **$Gd_{22}Ni_{21}$** and

releases CO_2 (Fig. S4b). The gas (0.2 mL) is collected with a sealing needle and injected into a gas chromatograph for analysis (Fig. S4b, S5). The experimental results of gas chromatography measurements show that the carbon dioxide in the air is negligible, and CO_2 molecules are released from compound **$Gd_{22}Ni_{21}$**. These experimental data suggest that CO_3^{2-} ions are in compound **$Gd_{22}Ni_{21}$**.

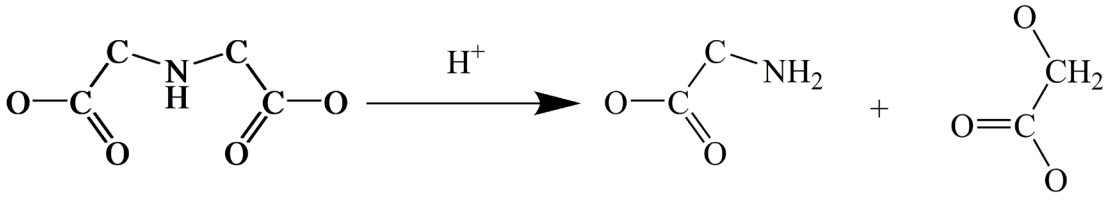

Fig. S2 The situ hydrolysis of H_2IDA.

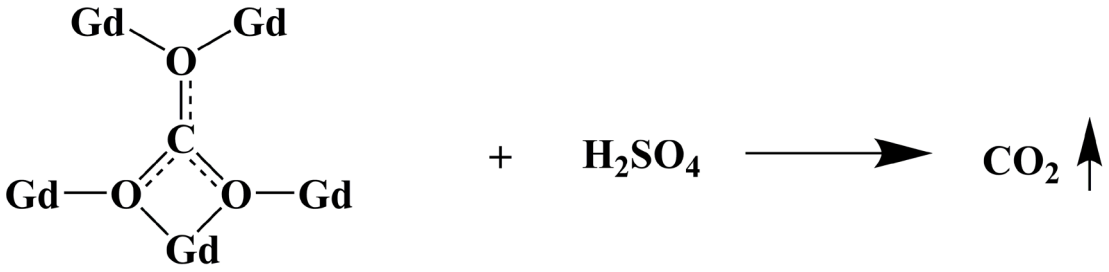

Fig. S3 The decomposition scheme of CO_2 from compound **$Gd_{22}Ni_{21}$** in the presence of concentrated H_2SO_4 (98 %; 80 μL).

Fig. S4 (a) The samples of compound **$Gd_{22}Ni_{21}$** immersed in water; (b) The samples of compound **$Gd_{22}Ni_{21}$** immersed in water with concentrated H_2SO_4 (80 μL).

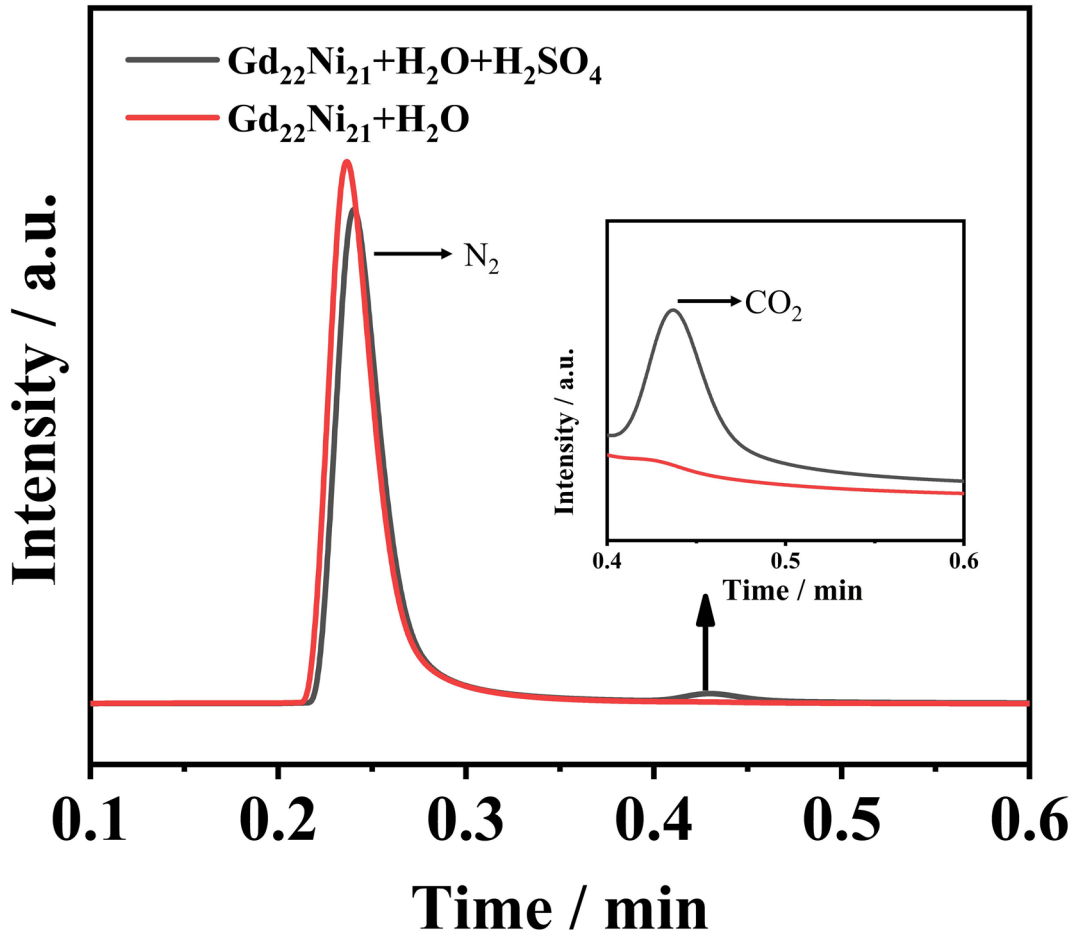

Fig. S5 Gas chromatography analyses of generated gases from the reaction of H_2O and solid samples of **$Gd_{22}Ni_{21}$** (red); concentrated H_2SO_4, H_2O and solid samples of **$Gd_{22}Ni_{21}$** (black). Inset: the enlarged drawing for 0.4 - 0.6 min.

Section 3. Crystal Structures

Crystal structure figures

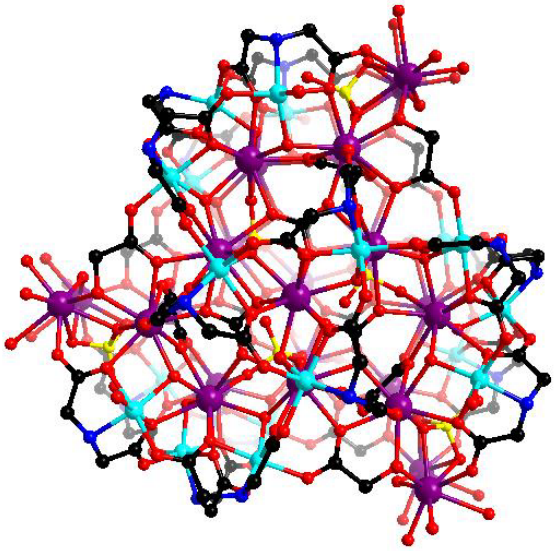

Fig. S6 The ball and stick view of cluster $\mathbf{Gd_{22}Ni_{21}}$. For clarity, free water molecules, H atoms and Cl^- ions were omitted.

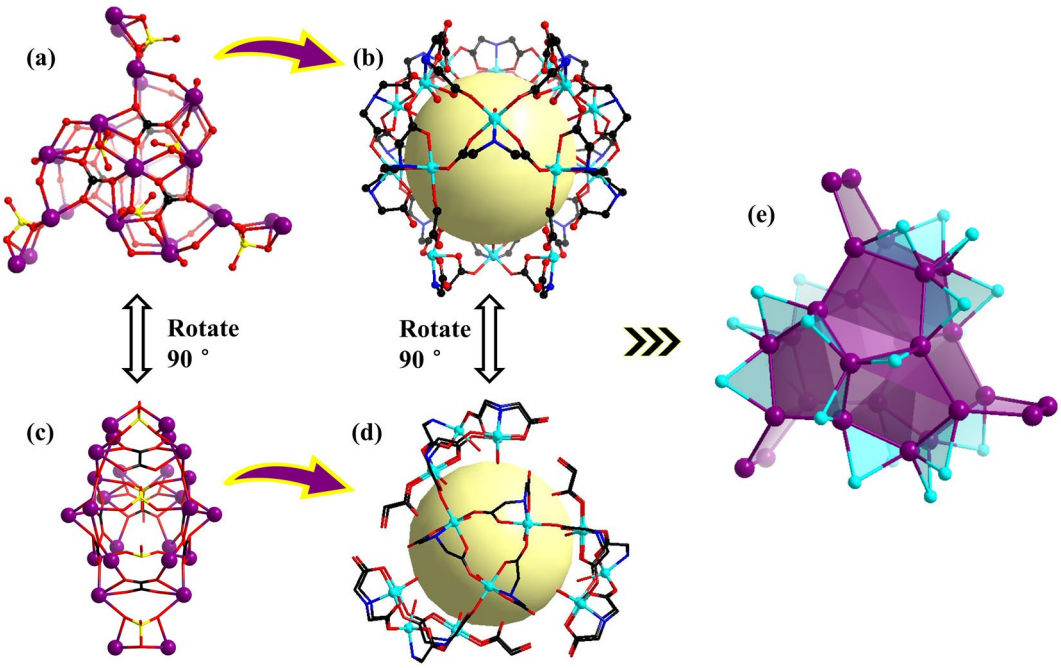

Fig. S7 The inner Ln-shell $\mathbf{Gd_{22}}$ (a), (c); the ball and stick view of external $\mathbf{Ni_{21}}$ shell (b), (d); the metal framework of $\mathbf{Gd_{22}Ni_{21}}$ (e).

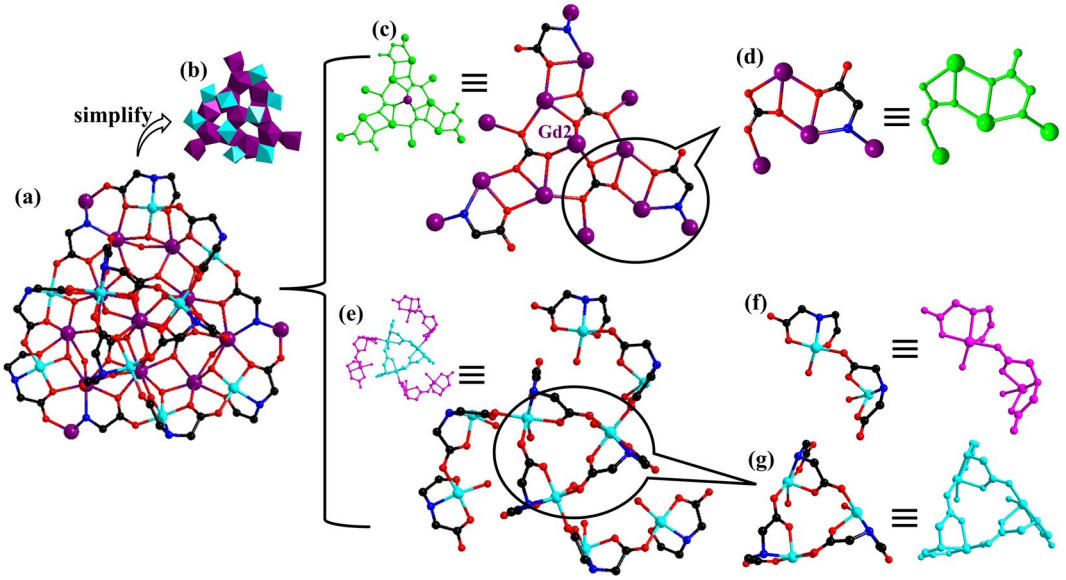

Fig. S8 Ball-and stick view of metal frame **$Gd_{13}Ni_9$** (a); the simplified view of **$Gd_{13}Ni_9$** (b); **Gd_{13}** (c); **Gd_4** (d); **$Ni_9(IDA)_9$** (e); **$Ni_2(IDA)_2$** (f); **$Ni_3(IDA)_3$** (g).

In order to clearly discuss the metal frame, propeller-like $Gd_{13}Ni_9$ can be disassembled into two components (Fig. S8): (i) $[Gd_{13}(CO_3)_3(HOCH_2COO)_3]^{30+}$ (**Gd_{13}**) Ln-shell comprised by three $[Gd_4(CO_3)(HOCH_2COO)]^{9+}$ (**Gd_4**) and one center Gd2 atom (Fig. S8c-d) via three CO_3^{2-} ions; (ii) Ni-shell, $Ni_9(IDA)_9$ constituted by three $Ni_2(IDA)_2$ groups and inner $Ni_3(IDA)_3$ via organic ligands IDA^{2-} (Fig. S8e-g). Then, **Gd_{13}** shell and **Ni_9** shell are linked to form propeller-shaped **$Gd_{13}Ni_9$** (Fig. S8a, b) unit via IDA^{2-} ligands again.

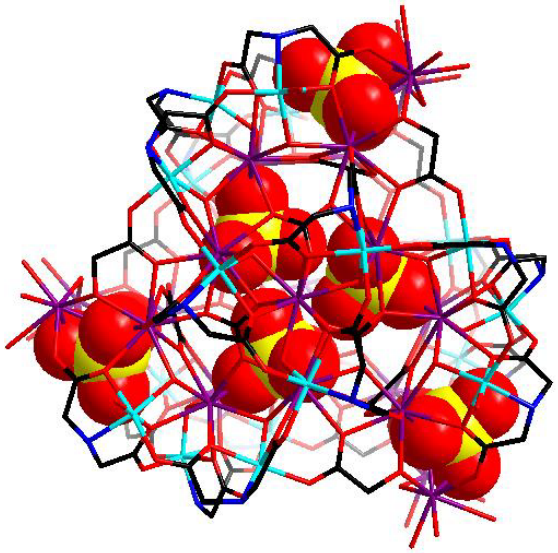

Fig. S9 The view of cluster **$Gd_{22}Ni_{21}$** templated by SO_4^{2-} and SO_3^{2-} anions. S, yellow; O, red.

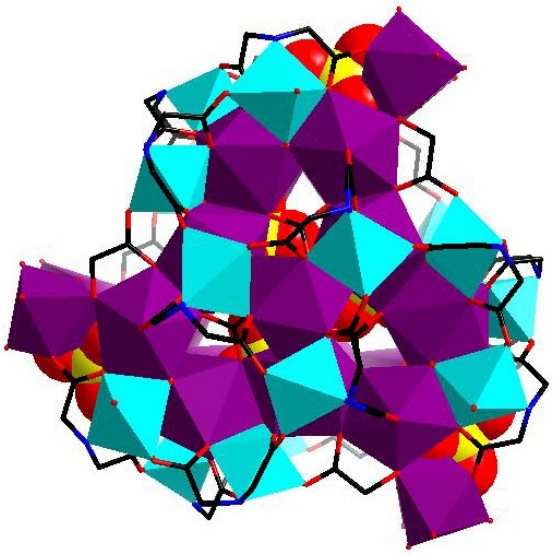

Fig. S10 The polyhedron view of cluster **$Gd_{22}Ni_{21}$** templated by SO_4^{2-} and SO_3^{2-} anions.

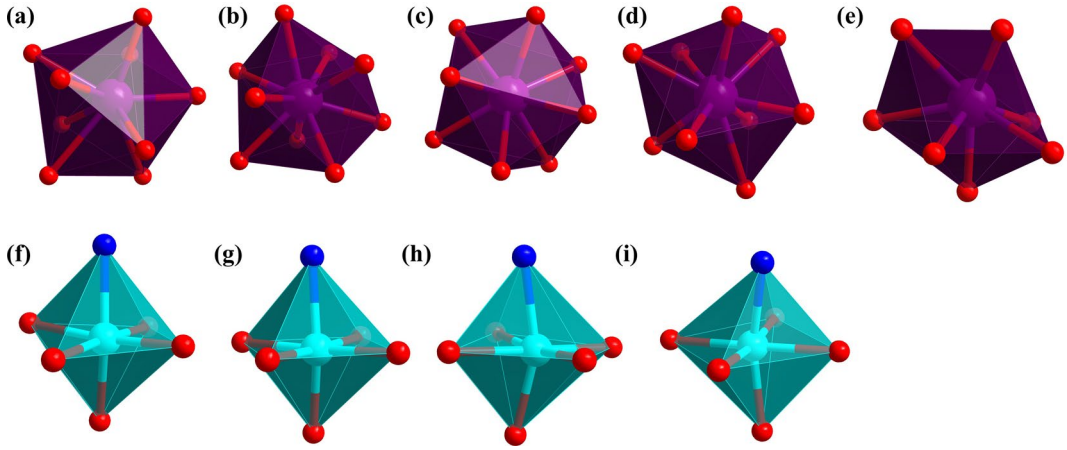

Fig. S11 Ball-and-stick of coordination environment of Gd1 (a), Gd2 (b), Gd3 (c), Gd4 (d), Gd5 (e), Ni1 (f), Ni2 (g), Ni3 (h), Ni4 (i).

The coordination mode of all metal ions (Gd^{3+} and Ni^{2+}) in cluster **$Gd_{22}Ni_{21}$** are exhibited in Fig. S11. **Gd1** is attached alongside nine O atoms (three oxygen atoms from carbonate ions, two O from μ_3-OH^-, one oxygen from SO_3^{2-}, and three oxygen from IDA^{2-} ligands). **Gd2** is linked by nine O-donors (three bridging oxygen from μ_3-OH^-, three oxygen atoms from CO_3^{2-}, as well as three oxygen from IDA^{2-} ligands). **Gd3** is coordinated by nine O-donors (two oxygen atoms from IDA^{2-} ligands, two oxygen atoms from one $HOCH_2COO^-$ ligand, two oxygen from oxalate, one oxygen from CO_3^{2-}, one oxygen from SO_3^{2-}, and one O from μ_3-OH^-. **Gd4** is connected with nine O atoms (one oxygen from SO_4^{2-}, two oxygen atoms from $HOCH_2COO^-$, one

bridging oxygen from μ_3-OH^-, two oxygen from oxalate, one oxygen atom from CO_3^{2-}, and the rest oxygen together from two IDA^{2-} ligands. While **Gd5** is seven-coordinated, connected to two oxygen from SO_4^{2-}, one O form $HOCH_2COO^-$, one oxygen atom from IDA^{2-} ligand, one oxygen atom from coordination H_2O, and the rest oxygen from μ_3-OH^- molecules. Beyond that, Ni^{2+} ions (Fig. S11e-f) are all six-coordinated with two different coordination modes. **Ni1**, **Ni2** and **Ni3** are connected to one N and five O donors (four oxygen atoms and one nitrogen atom from three IDA^{2-} ligands, and one O atom from one μ_3-OH^-). While **Ni4** is connected to one O-donor from μ_3-OH^-, one oxygen from water molecule, and the rest oxygen and one nitrogen atom from one IDA^{2-} ligand.

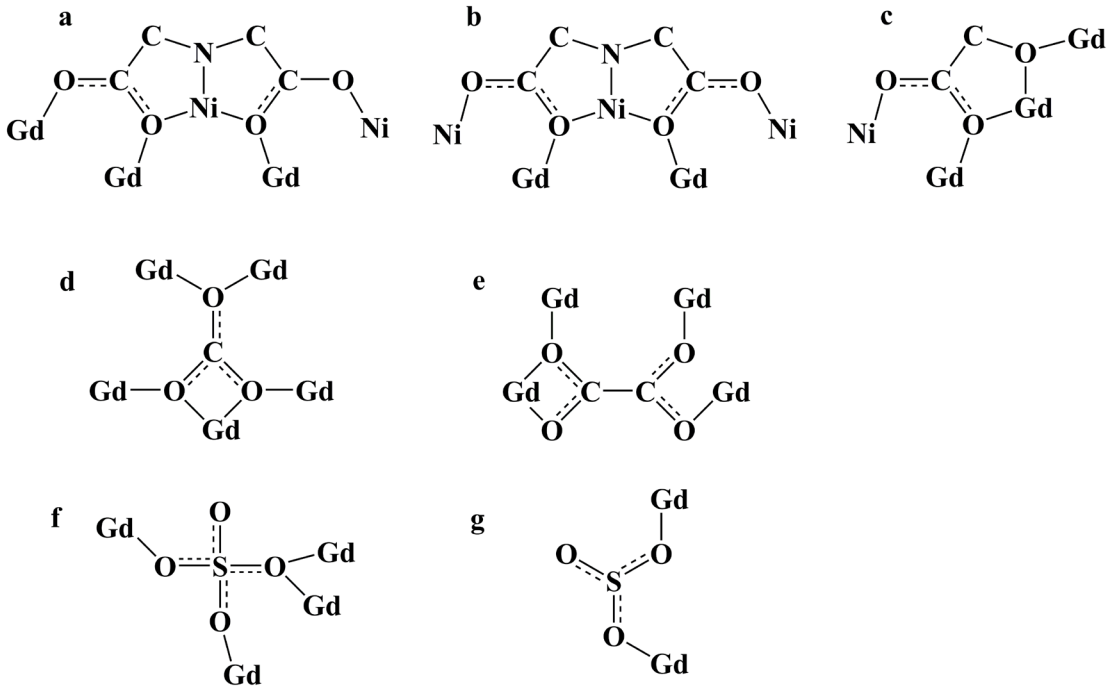

Fig. S12 The coordination modes of IDA^{2-} (a), (b); $HOCH_2COO^-$ (c); CO_3^{2-} (d); $C_2O_4^{2-}$ (e); SO_4^{2-} (f); SO_3^{2-} (g).

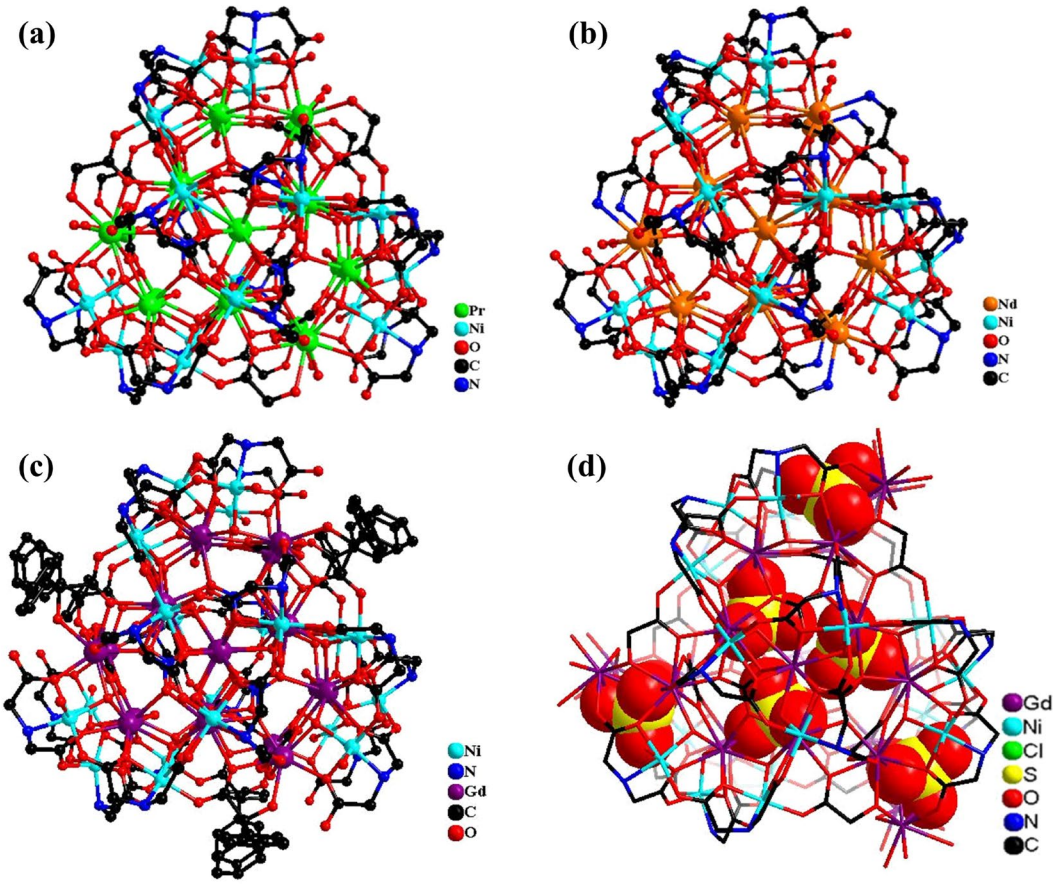

Fig. S13 Wires or Sticks views of $\{Ni_{21}Ln_{20}\}^3$ cages [Ln = Pr (a) and Nd (b)]; $\{Gd_{20}Ni_{21}\}^2$ cage (c); **$Gd_{22}Ni_{21}$** (d).

Section 4. Characterizations

PXRD

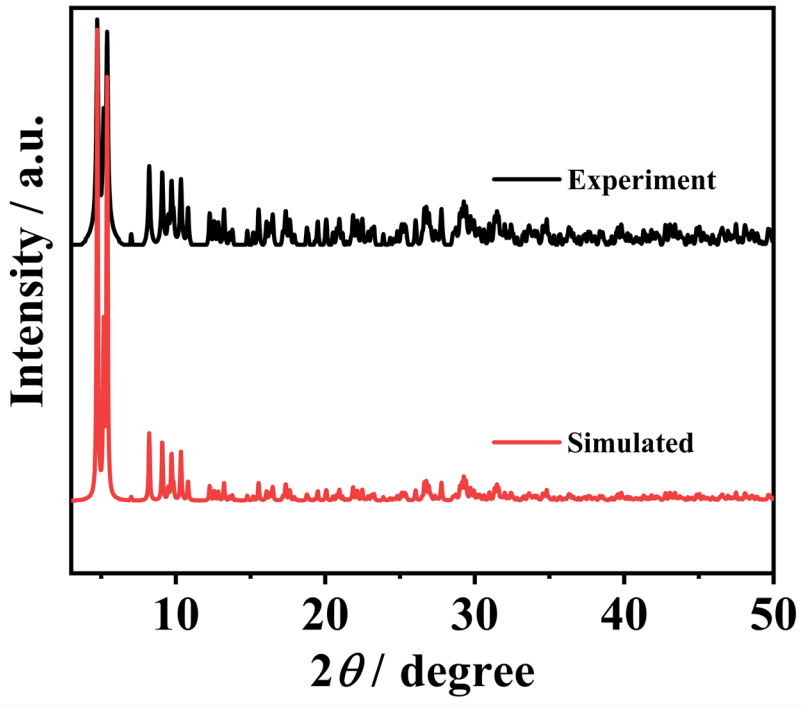

Fig. S14 The experimental and simulated PXRD patterns for compound **$Gd_{22}Ni_{21}$**.

For compound **$Gd_{22}Ni_{21}$**, the PXRD measurement was determined at room temperature. The experimental powder X-ray diffraction pattern of compound **$Gd_{22}Ni_{21}$** is consistent with the simulated pattern, showing the good purities of the sample phase.

FT-IR

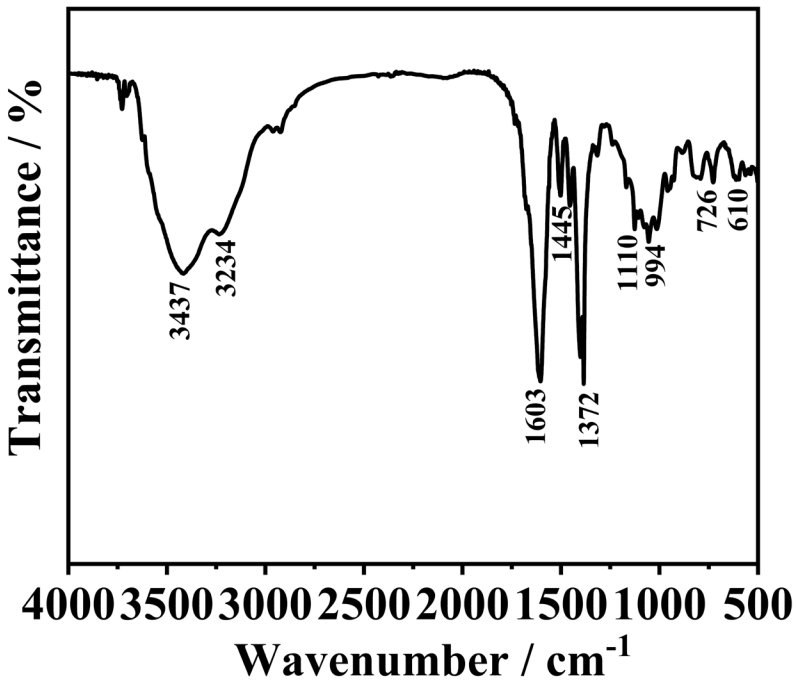

Fig. S15 The FT-IR of compound **$Gd_{22}Ni_{21}$**.

The strong peak at 3437 cm^{-1} can be ascribed to stretching vibration of O-H from water. Meanwhile, the characteristic peak at 3234 cm^{-1} is the stretching vibration of N-H. Moreover, the asymmetric stretching vibration peak on the carboxyl group corresponds to 1603 cm^{-1} and the symmetrical one appears at 1372 cm^{-1}. The peak at 1445 cm^{-1} is attributed to C=O stretching and bending vibrations, indicating the presence of CO_3^{2-} spices. The characteristic adsorption bands of SO_3^{2-} appear about at 610 cm^{-1}, whereas the bands in the regions of 1110-994 cm^{-1} can be attributed to SO_4^{2-}. In addition, the stretching vibration peak of the Ln-O bond appears at 726 cm^{-1} for compound **$Gd_{22}Ni_{21}$**. The occurrence of these characteristic adsorption bands is consistent with the similar compounds in the reported literatures.[5-8]

TGA

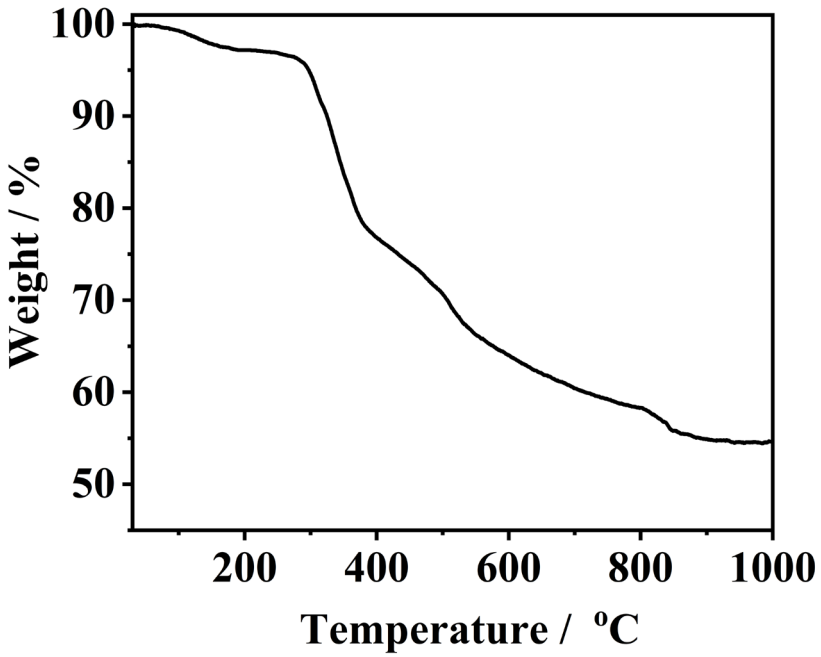

Fig. S16 TGA curve of compound **$Gd_{22}Ni_{21}$**.

TGA was performed (T = 25 - 1000 °C) in a N_2 atmosphere at a heating rate of 10 °C min^{-1} for compound **$Gd_{22}Ni_{21}$**. As shown in Fig. S16, the TGA diagram of **$Gd_{22}Ni_{21}$** displayed two weight loss phases. The first mass loss of 4.56 % in the temperature range of 25-290 °C can be ascribed to the loss of 12 coordination water and 15.5 free water molecules (the calculated value is 4.80 %). From 290 - 1000 °C, the weight loss corresponds to the decomposition of ligands and the collapse of the skeleton.

BVS

Table S2 Bond valence calculation (BVS) of compound **$Gd_{22}Ni_{21}$**.

		L	v	$\bar{v}$(BVS)
O1A	Gd1	2.339	2.58	1.11
	Gd2	2.392	0.44	
	Ni1	2.057	0.32	

O2A	Gd1 Gd3 Ni3	2.385 2.419 2.034	1.34 0.88 0.35	0.86
O3A	Gd3 Gd3 Ni2	2.384 2.384 2.049	1.46 1.46 0.33	1.08
O4A	Gd3 Gd4 Ni4	2.395 2.402 2.038	1.24 0.56 0.38	0.73
OH1	Gd3 Gd3	2.579 2.579	0.41 0.41	0.82
OH2	Gd4 Gd5	2.508 2.584	0.33 0.30	0.67

The relation between $\boldsymbol{L}$ and $\boldsymbol{v}$ is given by two curve segments:

$$For\ L \leq \bar{L},\ v = v_i\left(\frac{\bar{L}}{L}\right)^p \quad \textbf{(1)}$$

$$For\ \bar{L} \leq L \leq L_{MAX},\ v = v_i\frac{L_{MAX}-L}{L_{MAX}-\bar{L}} \quad \textbf{(2)}$$

$$p = \frac{\bar{L}}{L_{MAX}-\bar{L}} \quad \textbf{(3)}$$

where v_i is the ideal bond valence, defined as the quotient of the cationic charge by the coordination number (CN), and L_{MAX} is the upper limit of an atomic approach that will still be counted as an interatomic bond, so that CN is the number of anions at distances smaller than L_{MAX} from the cation. The average bond length, $\bar{\boldsymbol{L}}$, is the mean value determined for each coordination polyhedron in the structure at hand, so that its use enables us to adapt the curve to the bonding actually encountered. Should $\bar{\boldsymbol{L}}$ differ appreciably for two or more chemically identical but crystallographically different cations, a distinct curve is constructed and used for each one to obtain its bond valences.[23]

EDS

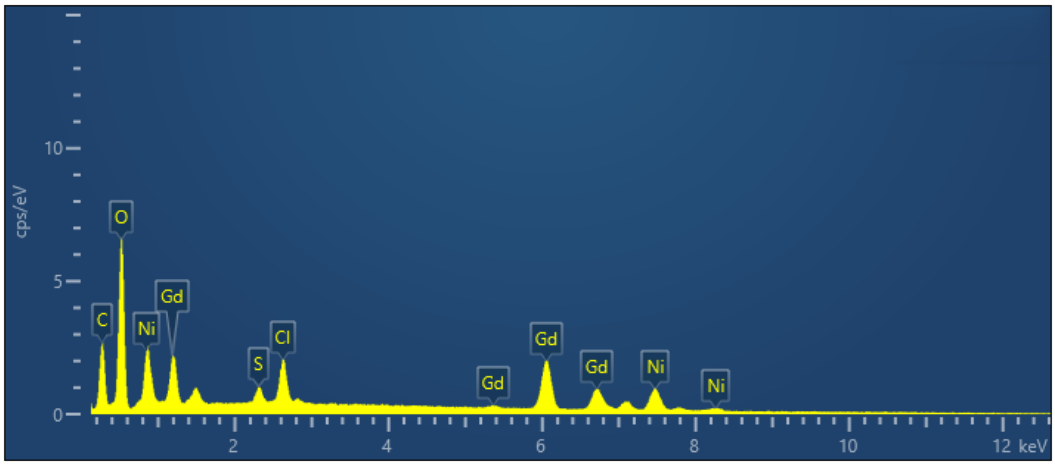

Fig. S17 The EDS measurement of compound **$Gd_{22}Ni_{21}$**.

Table S3 The Cl, Ni, S and Gd components of **$Gd_{22}Ni_{21}$** recorded from the EDS quantitative analyses.

Element	**Percentage by atomic / %**		
	1	2	average
Cl	3.76	3.89	3.82
Ni	3.50	3.68	3.59
S	1.06	1.15	1.11
Gd	1.60	1.65	1.62

ICP

Table S4 The ICP date of compound **$Gd_{22}Ni_{21}$**.

Content	**Gd (mmol / L)**	**Ni (mmol / L)**	**Gd / Ni (mol %)**
$Gd_{22}Ni_{21}$	0.01484	0.01456	1.0192

Section 5. Magnetic Studies

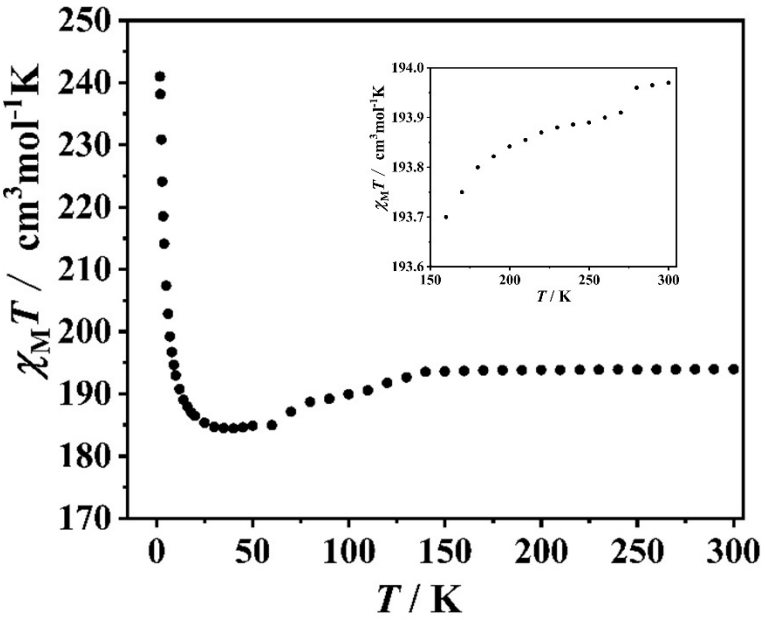

Fig. S18 Magnetic susceptibility versus temperature from 1.8 to 300 K under 1.0 kOe dc field for **$Gd_{22}Ni_{21}$**. Inset: magnetic susceptibility versus temperature from 150 to 300 K under 1.0 kOe dc field for **$Gd_{22}Ni_{21}$**.

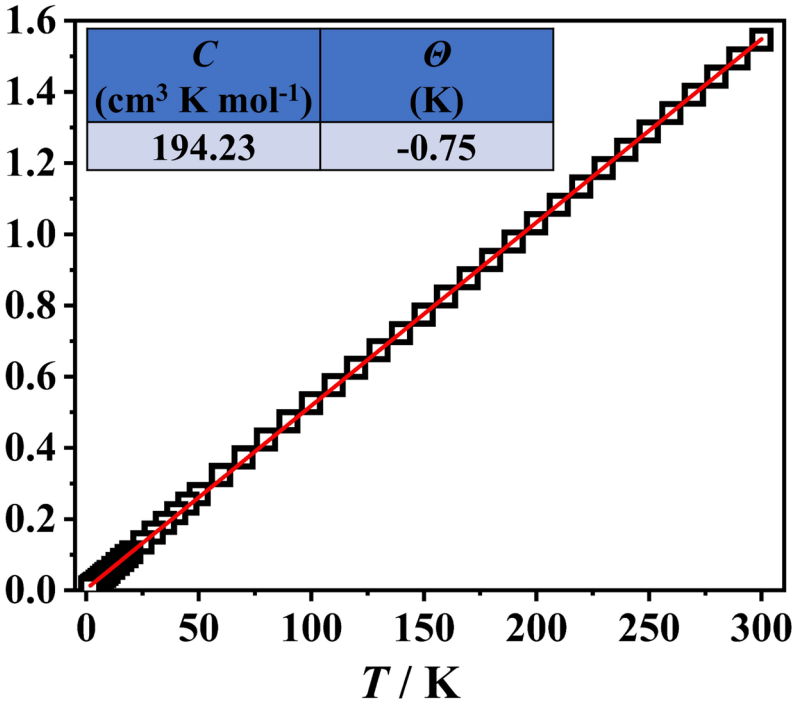

Fig. S19 χ_M^{-1} versus T plot of **$Gd_{22}Ni_{21}$**. The red line is fitting result with $\chi_M^{-1} = C / (T-\theta)$.

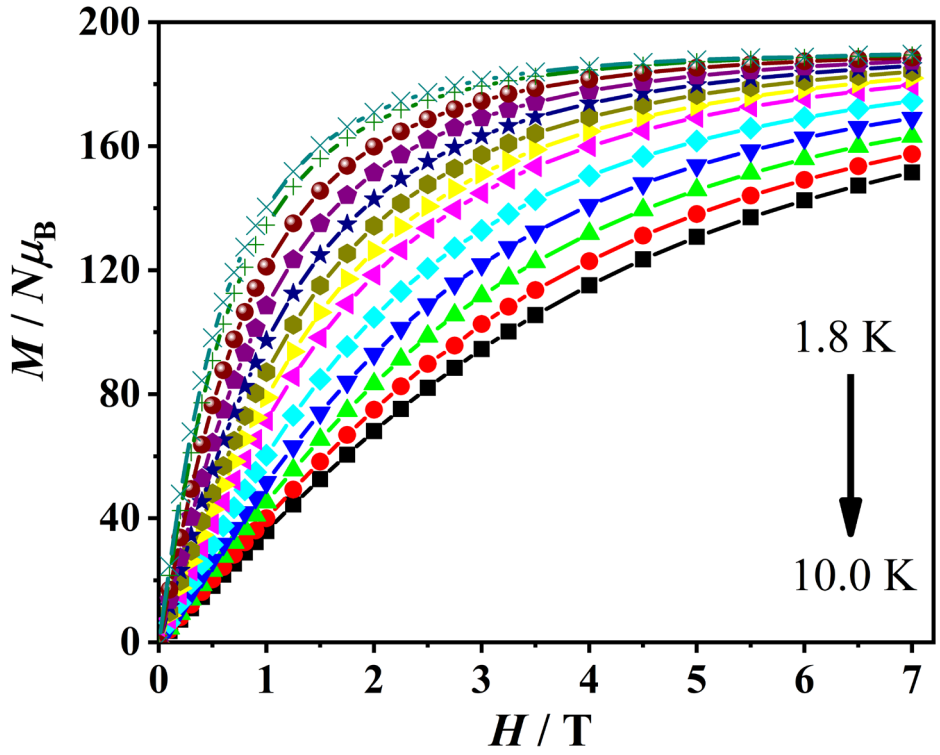

Fig. S20 The plots of field-dependent magnetization for **$Gd_{22}Ni_{21}$** (1.8-10 K).

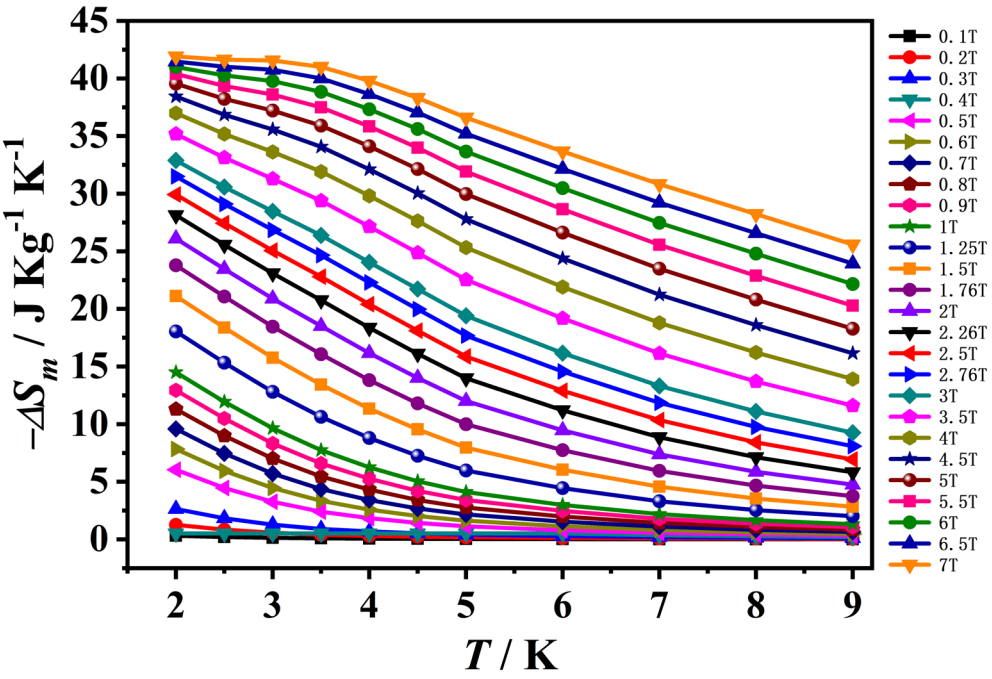

Fig. S21 Values of -ΔS_m calculated from the magnetization data for **$Gd_{22}Ni_{21}$**.

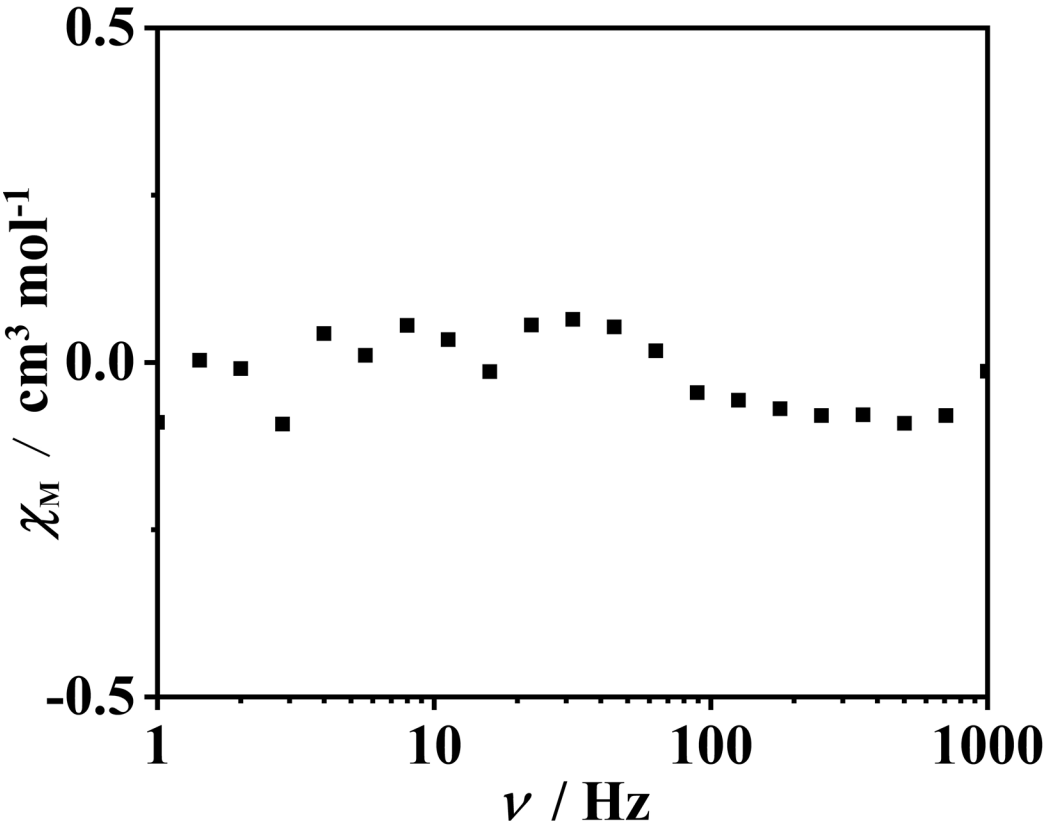

Fig. S22 Isothermal field sweep measurement performed on polycrystalline sample of **$Gd_{22}Ni_{21}$** at 1.8 K and 0 Oe.

Table S5 -ΔS_m (> 30 $J \cdot kg^{-1} \cdot K^{-1}$) for reported Gd-based polymetallic clusters.

Complexes	-ΔS_m ($J \cdot kg^{-1} \cdot K^{-1}$)	*T* (K)	ΔH (T)	*Ref.*
$\{Co_{12}Gd_{30}\}$	44.70	2.0	7.0	9a
$\{Ni_{64}Gd_{96}\}$	42.80	3.0	7	9b
$\{\mathbf{Ni_{21}Gd_{22}}\}$	41.90	2.0	7	This work
$\{Ni_{36}Gd_{102}\}$	41.30	2.0	7	10
$\{Co^{II}_{9}Co^{III}Gd_{42}\}$	41.26	2.0	7	11
$\{Ni_{64}Gd_{78}Si_{6}\}$	40.63	3.0	7	12
$\{Ni_{56}Gd_{52}\}$	40.10	2.0	7	13
$\{Ni_{10}Gd_{42}\}$	38.20	2.0	7	11
$\{Co^{II}Co^{III}_{6}Gd_{18}\}$	36.90	2.0	7	24
$\{Ni_{12}Gd_{36}\}$	36.30	3.0	7	14
$\{Ni_{44}Gd_{40}\}$	36.05	3.0	7	15
$\{Gd_{12}Mo_{4}\}$	35.30	3.0	7	16
$\{Ni_{21}Gd_{20}\}$	34.80	3.0	7	2
$\{Ni_{2}Gd_{2}\}$	34.40	4.5	7	17
$\{Mn_{4}Gd_{6}\}$	33.70	3.0	7	18
$\{Co_{4}Gd_{10}\}$	32.60	2.0	7	20
$\{Ni_{6}Gd_{6}\}$	32.00	3.0	7	21
$\{Cu_{5}Gd_{4}\}$	31.00	3.0	9	22

Section 6. Tables

Table S6 The CShM (Continuous Shape Measures) values of six-coordinated Ni ions in **$Gd_{22}Ni_{21}$**.

Refcode[a]	Ni1	Ni2	Ni3	Ni4
HP-6	33.414	33.403	31.989	32.393
PPY-6	24.262	23.847	25.285	21.465
OC-6	**1.067**	**0.968**	**0.825**	**1.494**
TPR-6	11.303	12.973	12.426	10.327
JPPY-6	28.256	27.587	28.98	25.235

[a]HP-6, hexagon; PPY-6, pentagonal pyramid; OC-6, octahedron; TPR-6, trigonal prism, JPPY-6, johnson pentagonal pyramid J2.

Table S7 The CShM (Continuous Shape Measures) values of seven-coordinated Gd ions in **$Gd_{22}Ni_{21}$**.

Refcode[a]	Gd5
HP-7	28.115
HPY-7	14.341
PBPY-7	8.199
COC-7	8.834
CTPR-7	**7.140**
JPBPY-7	9.319
JETPY-7	18.030

[a] HP-7, Heptagon; HPY-7, Hexagonal pyramid; PBPY-7, Pentagonal bipyramid; COC-7, Capped octahedron; CTPR-7, Capped trigonal prism; JPBPY-7, Johnson pentagonal bipyramid J13; JETPY-7, Johnson elongated triangular pyramid J7.

Table S8 The CShM (Continuous Shape Measures) values of nine-coordinated Gd ions in $\mathbf{Gd_{22}Ni_{21}}$.

Refcode[a]	Gd1	Gd2	Gd3	Gd4
EP-9	35.400	37.598	38.066	36.882
OPY-9	19.896	21.012	21.685	22.535
HBPY-9	19.191	21.328	21.24	18.801
JTC-9	14.848	16.98	15.721	15.994
JCCU-9	11.158	11.911	11.687	10.314
CCU-9	9.365	10.355	9.879	9.296
JCSAPR-9	2.975	2.547	2.508	1.612
CSAPR-9	1.887	1.267	1.047	0.767
JTCTPR-9	3.707	2.971	2.937	2.467
TCTPR-9	**1.375**	**0.118**	**0.454**	0.960
JTDIC-9	11.188	10.381	11.634	12.838
HH-9	11.902	13.888	12.092	12.097
MFF-9	2.204	1.992	1.625	**0.725**

[a]EP-9, enneagon; OPY-9, octagonal pyramid; HBPY-9, heptagonal bipyramid; JTC-9, Johnson triangular cupola J3; JCCU-9, capped cube J8; CCU-9, spherical-relaxed capped cube; JCSAPR-9, capped square antiprism J10; CSAPR-9, spherical capped square antiprism; JTCTPR-9, tricapped trigonal prism J51; TCTPR-9, spherical tricapped trigonal prism; JTDIC-9, tridiminished icosahedron J63; HH-9, hula-hoop; MFF-9, muffin.

Table S9 Selected bond lengths for compound $Gd_{22}Ni_{21}$ (Å)

Gd(1)-O(1A)	2.339(8)	Gd(3)-O(2B)#4	2.569(10)	Ni(2)-O(2)	2.036(10)
Gd(1)-O(2A)	2.385(8)	Gd(3)-O(1S)	2.577(11)	Ni(2)-O(2)#3	2.036(10)
Gd(1)-O(2S)	2.400(9)	Gd(4)-O(1B)	2.310(10)	Ni(2)-O(14)#3	2.048(9)
Gd(1)-O(1B)	2.469(9)	Gd(4)-N(5)	2.351(12)	Ni(2)-O(14)	2.048(9)
Gd(1)-O(15)	2.471(9)	Gd(4)-O(4A)#2	2.405(9)	Ni(2)-O(3A)	2.049(14)
Gd(1)-O(3B)	2.497(9)	Gd(4)-O(18)#2	2.409(19)	Ni(2)-N(4)	2.073(16)
Gd(1)-O(9)	2.504(8)	Gd(4)-O(6)#2	2.419(10)	Ni(3)-O(13)#3	1.999(9)
Gd(1)-O(2B)#1	2.609(9)	Gd(4)-O(4)#2	2.421(12)	Ni(3)-O(2A)	2.034(8)
Gd(1)-O(5)#2	2.697(9)	Gd(4)-O(17)#5	2.488(10)	Ni(3)-O(16)	2.042(11)
Gd(2)-O(1A)	2.392(9)	Gd(4)-O(7S)	2.507(17)	Ni(3)-O(9)	2.042(9)
Gd(2)-O(1A)#2	2.392(9)	Gd(4)-O(15)	2.510(10)	Ni(3)-O(11)	2.094(9)
Gd(2)-O(1A)#1	2.392(9)	Gd(5)-O(8W)	2.21(6)	Ni(3)-N(3)	2.100(10)
Gd(2)-O(3B)	2.428(8)	Gd(5)-O(6W)	2.23(3)	Ni(4)-O(4A)	2.038(9)
Gd(2)-O(3B)#2	2.428(8)	Gd(5)-O(3)	2.246(19)	Ni(4)-O(1)	2.042(9)
Gd(2)-O(3B)#1	2.428(8)	Gd(5)-O(7W)#6	2.27(6)	Ni(4)-O(4)	2.081(12)
Gd(2)-O(7)#1	2.467(8)	Gd(5)-N(5)#1	2.473(14)	Ni(4)-O(12)	2.086(11)
Gd(2)-O(7)	2.467(8)	Gd(5)-O(7S)#1	2.53(2)	Ni(4)-N(1)	2.093(12)
Gd(2)-O(7)#2	2.467(9)	Gd(5)-O(6S)#1	2.57(2)	Ni(4)-O(1W)	2.095(10)
Gd(3)-O(3A)	2.384(8)	Gd(5)-O(7W)	2.68(6)	S(1A)-O(3S)	1.44(3)
Gd(3)-O(4A)#3	2.395(8)	Ni(1)-O(10)	2.006(9)	S(1A)-O(2S)#3	1.532(10)
Gd(3)-O(2A)#3	2.419(9)	Ni(1)-O(5)#2	2.031(9)	S(1A)-O(2S)	1.532(10)
Gd(3)-O(11)#3	2.499(8)	Ni(1)-O(7)#2	2.040(9)	S(1A)-O(1S)	1.626(19)
Gd(3)-O(14)	2.500(9)	Ni(1)-O(1A)	2.057(8)	S(1B)-O(4S)	1.49(5)
Gd(3)-O(17)	2.503(10)	Ni(1)-O(8)	2.070(9)	S(1B)-O(2S)#3	1.493(16)
Gd(3)-O(1)#3	2.551(8)	Ni(1)-N(2)#2	2.084(11)	S(1B)-O(2S)	1.493(16)
O(1A)-Gd(1)-O(2A)	119.4(3)	O(2S)-Gd(1)-O(15)	98.0(4)	O(2A)-Gd(1)-O(9)	68.2(3)
O(1A)-Gd(1)-O(2S)	132.6(3)	O(1B)-Gd(1)-O(15)	67.7(3)	O(2S)-Gd(1)-O(9)	140.2(3)
O(2A)-Gd(1)-O(2S)	72.0(3)	O(1A)-Gd(1)-O(3B)	69.9(3)	O(1B)-Gd(1)-O(9)	131.9(3)
O(1A)-Gd(1)-O(1B)	108.5(3)	O(2A)-Gd(1)-O(3B)	146.9(3)	O(15)-Gd(1)-O(9)	75.5(3)
O(2A)-Gd(1)-O(1B)	132.1(3)	O(2S)-Gd(1)-O(3B)	79.3(3)	O(3B)-Gd(1)-O(9)	138.6(3)
O(2S)-Gd(1)-O(1B)	76.4(3)	O(1B)-Gd(1)-O(3B)	52.0(3)	O(1A)-Gd(1)-O(2B)#1	71.7(3)
O(1A)-Gd(1)-O(15)	128.1(3)	O(15)-Gd(1)-O(3B)	118.7(3)	O(2A)-Gd(1)-O(2B)#1	67.5(3)
O(2A)-Gd(1)-O(15)	82.0(3)	O(1A)-Gd(1)-O(9)	71.6(3)	O(2S)-Gd(1)-O(2B)#1	72.3(3)
O(1B)-Gd(1)-O(2B)#1	133.4(3)	O(3B)#1-Gd(2)-O(7)	96.1(3)	O(3A)-Gd(3)-O(1S)	70.2(4)
O(15)-Gd(1)-O(2B)#1	149.6(3)	O(7)#1-Gd(2)-O(7)	72.0(3)	O(4A)#3-Gd(3)-O(1S)	134.9(4)
O(3B)-Gd(1)-O(2B)#1	88.4(3)	O(1A)-Gd(2)-O(7)#2	70.7(3)	O(2A)#3-Gd(3)-O(1S)	73.2(4)

O(9)-Gd(1)-O(2B)#1	93.4(3)	O(1A)#2-Gd(2)-O(7)#2	67.3(3)	O(11)#3-Gd(3)-O(1S)	140.2(4)
O(1A)-Gd(1)-O(5)#2	63.1(3)	O(1A)#1-Gd(2)-O(7)#2	131.1(3)	O(14)-Gd(3)-O(1S)	94.3(4)
O(2A)-Gd(1)-O(5)#2	133.8(3)	O(3B)-Gd(2)-O(7)#2	96.1(3)	O(17)-Gd(3)-O(1S)	76.5(5)
O(2S)-Gd(1)-O(5)#2	144.5(3)	O(3B)#2-Gd(2)-O(7)#2	137.4(3)	O(1)#3-Gd(3)-O(1S)	139.6(4)
O(1B)-Gd(1)-O(5)#2	68.1(3)	O(3B)#1-Gd(2)-O(7)#2	144.4(3)	O(2B)#4-Gd(3)-O(1S)	77.3(4)
O(15)-Gd(1)-O(5)#2	68.6(3)	O(7)#1-Gd(2)-O(7)#2	72.0(3)	O(1B)-Gd(4)-O(4A)#2	74.8(3)
O(3B)-Gd(1)-O(5)#2	79.3(3)	O(7)-Gd(2)-O(7)#2	72.0(3)	O(1B)-Gd(4)-O(18)#2	75.9(5)
O(9)-Gd(1)-O(5)#2	70.3(3)	O(3A)-Gd(3)-O(4A)#3	118.3(4)	O(4A)#2-Gd(4)-O(18)#2	132.0(4)
O(2B)#1-Gd(1)-O(5)#2	134.7(3)	O(3A)-Gd(3)-O(2A)#3	123.2(4)	O(1B)-Gd(4)-O(6)#2	85.7(3)
O(1A)-Gd(2)-O(1A)#2	119.93(2)	O(4A)#3-Gd(3)-O(2A)#3	118.4(3)	O(4A)#2-Gd(4)-O(6)#2	74.1(3)
O(1A)-Gd(2)-O(1A)#1	119.927(19)	O(3A)-Gd(3)-O(11)#3	128.8(4)	O(18)#2-Gd(4)-O(6)#2	139.6(5)
O(1A)#2-Gd(2)-O(1A)#1	119.927(19)	O(4A)#3-Gd(3)-O(11)#3	72.3(3)	O(1B)-Gd(4)-O(4)#2	142.9(3)
O(1A)-Gd(2)-O(3B)	70.2(3)	O(2A)#3-Gd(3)-O(11)#3	67.4(3)	O(4A)#2-Gd(4)-O(4)#2	68.2(3)
O(1A)#2-Gd(2)-O(3B)	73.8(3)	O(3A)-Gd(3)-O(14)	66.9(4)	O(18)#2-Gd(4)-O(4)#2	132.8(6)
O(1A)#1-Gd(2)-O(3B)	132.7(3)	O(4A)#3-Gd(3)-O(14)	130.5(3)	O(6)#2-Gd(4)-O(4)#2	81.7(4)
O(1A)-Gd(2)-O(3B)#2	132.7(3)	O(2A)#3-Gd(3)-O(14)	74.3(3)	O(1B)-Gd(4)-O(17)#5	71.2(4)
O(1A)#2-Gd(2)-O(3B)#2	70.2(3)	O(11)#3-Gd(3)-O(14)	70.3(3)	O(4A)#2-Gd(4)-O(17)#5	68.4(3)
O(1A)#1-Gd(2)-O(3B)#2	73.8(3)	O(3A)-Gd(3)-O(17)	68.6(4)	O(18)#2-Gd(4)-O(17)#5	66.6(4)
O(3B)-Gd(2)-O(3B)#2	69.6(3)	O(4A)#3-Gd(3)-O(17)	68.2(3)	O(6)#2-Gd(4)-O(17)#5	139.8(3)
O(1A)-Gd(2)-O(3B)#1	73.8(3)	O(2A)#3-Gd(3)-O(17)	139.4(3)	O(4)#2-Gd(4)-O(17)#5	97.1(4)
O(1A)#2-Gd(2)-O(3B)#1	132.7(3)	O(11)#3-Gd(3)-O(17)	140.1(3)	O(1B)-Gd(4)-O(7S)	129.9(5)
O(1A)#1-Gd(2)-O(3B)#1	70.2(3)	O(14)-Gd(3)-O(17)	134.9(3)	O(4A)#2-Gd(4)-O(7S)	111.9(6)
O(3B)-Gd(2)-O(3B)#1	69.6(3)	O(3A)-Gd(3)-O(1)#3	69.6(4)	O(18)#2-Gd(4)-O(7S)	63.3(7)
O(3B)#2-Gd(2)-O(3B)#1	69.6(3)	O(4A)#3-Gd(3)-O(1)#3	65.0(3)	O(6)#2-Gd(4)-O(7S)	144.4(5)
O(1A)-Gd(2)-O(7)#1	131.1(3)	O(2A)#3-Gd(3)-O(1)#3	135.0(3)	O(4)#2-Gd(4)-O(7S)	69.6(6)
O(1A)#2-Gd(2)-O(7)#1	70.7(3)	O(11)#3-Gd(3)-O(1)#3	72.6(3)	O(17)#5-Gd(4)-O(7S)	66.8(5)
O(1A)#1-Gd(2)-O(7)#1	67.3(3)	O(14)-Gd(3)-O(1)#3	73.6(3)	O(1B)-Gd(4)-O(15)	69.6(3)
O(3B)-Gd(2)-O(7)#1	144.4(3)	O(17)-Gd(3)-O(1)#3	85.3(4)	O(4A)#2-Gd(4)-O(15)	135.5(3)
O(3B)#2-Gd(2)-O(7)#1	96.1(3)	O(3A)-Gd(3)-O(2B)#4	138.7(4)	O(18)#2-Gd(4)-O(15)	62.5(4)
O(3B)#1-Gd(2)-O(7)#1	137.4(3)	O(4A)#3-Gd(3)-O(2B)#4	69.7(3)	O(6)#2-Gd(4)-O(15)	77.5(3)
O(1A)-Gd(2)-O(7)	67.3(3)	O(2A)#3-Gd(3)-O(2B)#4	67.7(3)	O(4)#2-Gd(4)-O(15)	139.5(4)
O(1A)#2-Gd(2)-O(7)	131.1(3)	O(11)#3-Gd(3)-O(2B)#4	92.4(3)	O(17)#5-Gd(4)-O(15)	121.1(3)
O(1A)#1-Gd(2)-O(7)	70.7(3)	O(14)-Gd(3)-O(2B)#4	141.9(3)	O(7S)-Gd(4)-O(15)	111.2(6)
O(3B)-Gd(2)-O(7)	137.4(3)	O(17)-Gd(3)-O(2B)#4	79.8(3)	O(10)-Ni(1)-O(5)#2	92.7(4)
O(3B)#2-Gd(2)-O(7)	144.4(3)	O(1)#3-Gd(3)-O(2B)#4	134.7(3)	O(10)-Ni(1)-O(7)#2	172.3(3)
O(5)#2-Ni(1)-O(7)#2	91.3(4)	O(4A)-Ni(4)-O(4)	82.2(4)	O(6S)#1-Gd(5)-O(7W)	63.2(13)
O(10)-Ni(1)-O(1A)	100.5(4)	O(1)-Ni(4)-O(4)	97.0(4)	O(3S)-S(1A)-O(2S)#3	114.1(8)
O(5)#2-Ni(1)-O(1A)	80.9(3)	O(4A)-Ni(4)-O(12)	103.7(4)	O(3S)-S(1A)-O(2S)	114.1(8)

O(7)#2-Ni(1)-O(1A)	86.6(3)	O(1)-Ni(4)-O(12)	88.0(4)	O(2S)#3-S(1A)-O(2S)	100.1(9)
O(10)-Ni(1)-O(8)	87.2(4)	O(4)-Ni(4)-O(12)	172.8(4)	O(3S)-S(1A)-O(1S)	101.5(12)
O(5)#2-Ni(1)-O(8)	176.1(4)	O(4A)-Ni(4)-O(1W)	98.6(4)	O(2S)#3-S(1A)-O(1S)	113.8(6)
O(7)#2-Ni(1)-O(8)	89.3(4)	O(1)-Ni(4)-O(1W)	175.6(5)	O(2S)-S(1A)-O(1S)	113.8(6)
O(1A)-Ni(1)-O(8)	95.2(4)	O(4)-Ni(4)-O(1W)	87.3(5)	O(4S)-S(1B)-O(2S)#3	112.7(16)
O(2)-Ni(2)-O(2)#3	87.5(7)	O(12)-Ni(4)-O(1W)	87.8(4)	O(2S)#3-S(1B)-O(2S)	103.7(15)
O(2)-Ni(2)-O(14)#3	91.4(4)	O(8W)-Gd(5)-O(6W)	137(2)	O(6S)-S(2)-O(7S)	106.8(13)
O(2)#3-Ni(2)-O(14)#3	176.9(4)	O(8W)-Gd(5)-O(3)	78.0(17)	O(6S)-S(2)-O(7S)#3	106.8(13)
O(2)-Ni(2)-O(14)	176.9(4)	O(6W)-Gd(5)-O(3)	145.0(16)	O(7S)-S(2)-O(7S)#3	96.2(18)
O(2)#3-Ni(2)-O(14)	91.4(4)	O(8W)-Gd(5)-O(7W)#6	68(2)	O(6S)-S(2)-O(5S)	106.1(18)
O(14)#3-Ni(2)-O(14)	89.4(5)	O(6W)-Gd(5)-O(7W)#6	73(2)	O(7S)-S(2)-O(5S)	119.9(12)
O(2)-Ni(2)-O(3A)	100.9(4)	O(3)-Gd(5)-O(7W)#6	137.8(15)	O(7S)#3-S(2)-O(5S)	119.9(12)
O(2)#3-Ni(2)-O(3A)	100.9(4)	O(8W)-Gd(5)-O(7S)#1	136.4(16)	Gd(5)#5-O(6S)-Gd(5)#2	95.5(11)
O(14)#3-Ni(2)-O(3A)	82.2(4)	O(6W)-Gd(5)-O(7S)#1	74.8(17)	Gd(4)-O(7S)-Gd(5)#2	105.0(6)
O(14)-Ni(2)-O(3A)	82.2(4)	O(3)-Gd(5)-O(7S)#1	75.4(8)	Gd(1)-O(1A)-Gd(2)	112.6(3)
O(13)#3-Ni(3)-O(2A)	101.7(4)	O(7W)#6-Gd(5)-O(7S)#1	146.7(15)	Gd(1)-O(2A)-Gd(3)#3	118.6(3)
O(13)#3-Ni(3)-O(16)	89.5(4)	O(8W)-Gd(5)-O(6S)#1	145.0(18)	Gd(3)-O(3A)-Gd(3)#3	115.9(6)
O(2A)-Ni(3)-O(16)	97.1(4)	O(6W)-Gd(5)-O(6S)#1	71.0(15)	Gd(3)#3-O(4A)-Gd(4)#1	114.8(3)
O(13)#3-Ni(3)-O(9)	173.7(4)	O(3)-Gd(5)-O(6S)#1	78.1(8)	Gd(1)-O(15)-Gd(4)	107.9(4)
O(2A)-Ni(3)-O(9)	84.6(3)	O(7W)#6-Gd(5)-O(6S)#1	118.1(15)	Gd(4)#4-O(17)-Gd(3)	108.2(3)
O(16)-Ni(3)-O(9)	89.2(4)	O(7S)#1-Gd(5)-O(6S)#1	58.8(7)	Gd(3)#5-O(2B)-Gd(1)#2	105.8(3)
O(13)#3-Ni(3)-O(11)	93.4(4)	O(8W)-Gd(5)-O(7W)	83(2)	Gd(2)-O(3B)-Gd(1)	106.2(3)
O(2A)-Ni(3)-O(11)	82.7(3)	O(6W)-Gd(5)-O(7W)	114.3(18)	Gd(5)#3-O(6W)-Gd(5)	117.0(3)
O(16)-Ni(3)-O(11)	177.0(4)	O(3)-Gd(5)-O(7W)	62.7(12)	Gd(5)#7-O(7W)-Gd(5)	149.0(2)

References

(1) (a) Guo, F.-S.; Chen, Y.-C.; Liu, J.-L.; Leng, J.-D.; Meng, Z.-S.; Vra´ bel, P.; Orenda´, M.; Tong, M.-L. A large cryogenic magnetocaloric effect exhibited at low field by a 3D ferromagnetically coupled $Mn^{(II)}$–$Gd^{(III)}$ framework material. *Chem. Commun*. **2012**, *48*, 12219-12221. (b) Zhao, X.; Xiao, B.; Fletcher, A. J.; Thomas, K. M.; Bradshaw, D.; Rosseinsky, M. J. Hysteretic Adsorption and Desorption of Hydrogen by Nanoporous Metal-Organic Frameworks. *Science* **2004**, *306*, 1012-1015. (c) Kong, X.-J., Ren, Y.-P., Long, L.-S., Zheng, Z., Huang, R.-B., Zheng, L.-S. A Keplerate Magnetic Cluster Featuring an Icosidodecahedron of $Ni^{(II)}$ Ions Encapsulating a Dodecahedron of $La^{(III)}$ Ions. *J. Am. Chem. Soc.* **2007**, 129, 7016–7017. (d) Karotsis, G., Evangelisti, M., Dalgarno, S., Brechin, E. A Calix[4]arene 3d/4f Magnetic Cooler. *Angew. Chem., Int. Ed.* **2009**, *48*, 9928–9931.

(2) Chen, W.-P.; Singleton, J.; Qin, L.; Camón, A.; Engelhardt, L.; Luis, F.; Winpenny, R. E. P.; Zheng, Y.-Z. Quantum Monte Carlo Simulations of a Giant $\{Ni_{21}Gd_{20}\}$ Cage with a $S = 91$ Spin Ground State. *Nat. Comm*. **2018**, *9*, 1-6.

(3) Kong, X.-J.; Ren, Y.-P.; Long, L.-S.; Zheng, Z.; Nichol, G.; Huang, R.-B.; Zheng, L.-S. Dual Shell-Like Magnetic Clusters Containing Ni^{II} and Ln^{III} (Ln = La, Pr, and Nd) Ions. *Inorg. Chem.* **2008**, *47*, 2728-2739.

(4) Cui, C.-H.; He, X.-X.; Lin, Q.-F.; Luo, X.-M.; Xu, Y. Two Nanosized Cage-Like $Ln_{20}Ni_{21}$ Clusters Exhibiting Antiferromagnetic Properties. *Inorg. Chem. Commun.* **2018**, *90*, 101-104.

(5) Rao, K. P.; Rao, C. N. R. Coordination Polymers and Hybrid Networks of Different Dimensionalities Formed by Metal Sulfites. *Inorg. Chem.* **2007**, *46*, 2511-2518.

(6) Giauque, W. F.; MacDougall, D. P. Attainment of Temperatures Below 1° Absolute by Demagnetization of $Gd_2(SO_4)_3 \cdot 8H_2O$. *Phys. Rev.* **1933**, *43*, 768.

(7) Papatriantafyllopoulou, C.; Manessi-Zoupa, E.; Escuer, A.; Perlepes, S. P. The Sulfate Ligand as a Promising "Player" in 3d-metal Cluster Chemistry. *Inorg. Chim. Acta.* **2009**, *362*, 634-650.

(8) Rao, C. N. R.; Natarajan, S.; Vaidhyanathan, R. Metal Carboxylates with Open Architectures. *Angew. Chem., Int. Ed.* **2004**, *43*, 1466-1496.

(9) (a) Lun, H.-J.; Xu, L.; Kong, X.-J.; Long, L.-S.; Zheng, L.-S. A High-Symmetry Double-Shell $Gd_{30}Co_{12}$ Cluster Exhibiting a Large Magnetocaloric Effect. *Inorg. Chem.* **2021**, DOI: 10.1021/acs.inorgchem.1c00993. (b) Chen, W.-P.; Liao, P.-Q.; Yu, Y.; Zheng, Z.; Chen, X.-M.; Zheng, Y.-Z. A Mixed-Ligand Approach for a Gigantic and Hollow Heterometallic Cage $\{Ni_{64}RE_{96}\}$ for Gas Separation and Magnetic Cooling Applications. *Angew. Chem., Int. Ed.* **2016**, *55*, 9375-9379.

(10) Chen, W.-P.; Liao, P.-Q.; Jin, P.-B.; Zhang, L.; Ling, B.-K.; Wang, S.-C.; Chan, Y.-T.; Chen, X.-M.; Zheng, Y.-Z. The Gigantic $\{Ni_{36}Gd_{102}\}$ Hexagon: a Sulfate-Templated "Star-of-David" for Photocatalytic CO_2 Reduction and Magnetic Cooling. *J. Am. Chem. Soc.* **2020**, *142*, 4663-4670.

(11) Peng, J.-B.; Zhang, Q.-C.; Kong, X.-J.; Zheng, Y.-Z.; Ren, Y.-P.; Long, L.-S.; Huang, R.-B.; Zheng, L.-S.; Zheng, Z.-P. High-Nuclearity 3d-4f Clusters as Enhanced Magnetic Coolers and Molecular Magnets. *J. Am. Chem. Soc.* **2012**, *134*, 3314-3317.

(12) Lin, Q.-F.; Li, J.; Luo, X.-M.; Cui, C.-H.; Song, Y., Xu, Y. Incorporation of Silicon-Oxygen Tetrahedron into Novel High-Nuclearity Nanosized 3d-4f Heterometallic Clusters. *Inorg. Chem.* **2018**, *57*, 4799-4802.

(13) Liu, D.-P.; Lin, X.-P.; Zhang, H.; Zheng, X.-Y.; Zhuang, G.-L.; Kong, X.-J.; Long, L.-S.; Zheng, L.-S. Magnetic Properties of a Single-Molecule Lanthanide-Transition-Metal Compound Containing 52 Gadolinium and 56 Nickel At-oms. *Angew. Chem., Int. Ed.* **2016**, *55*, 4532-4536.

(14) Peng, J.-B.; Zhang, Q.-C.; Kong, X.-J.; Ren, Y.-P.; Long, L.-S.; Huang, R.-B.; Zheng, L.-S.; Zheng, Z.-P. A 48-Metal Cluster Exhibiting a Large Magnetocaloric Effect. *Angew. Chem., Int. Ed.* **2011**, *50*, 10649-10652.

(15) Evangelisti, M.; Roubeau, O.; Palacios, E.; Camón, A.; Hooper, T. N.; Brechin, E. K.; Alonso, J. J. Cryogenic Magnetocaloric Effect in a Ferromagnetic Molecular Dimer. *Angew. Chem., Int. Ed.* **2011**, *50*, 6606-6609.

(16) Zheng, Y.; Zhang, Q.-C.; Long, L.-S.; Huang, R.-B.; Müller, A.; Schnack, J.; Zheng, Z.-P. Molybdate Templated Assembly of $Ln_{12}Mo_4$-Type Clusters (Ln= Sm, Eu, Gd) Containing a Truncated Tetrahedron Core. *Chem. Commun.* **2013**, *49*, 36-38.

(17) Wang, P.; Shannigrahi, S.; Yakovlev, N. L.; Andy Hor, T. S. Facile Self-Assembly of Intermetallic $\{Ni_2Gd_2\}$ Cubane Aggregate for Magnetic Refrigeration. *Chem. Asian J.* **2013**, *8*, 2943-2946.

(18) Zheng, Y.-Z.; Pineda, E. M.; Helliwell, M.; Winpenny, R. E. P. Mn^{II}-Gd^{III} Phosphonate Cages with a Large Magnetocaloric Effect. *Chem. Eur. J.* **2012**, *18*, 4161-4165.

(19) Zheng, Y.-Z.; Evangelisti, M.; Tuna, F.; Winpenny, R. E. P. Co-Ln Mixed-Metal Phosphonate Grids and Cages as Molecular Magnetic Refrigerants. *J. Am. Chem. Soc.* **2012**, *134*, 1057-1065.

(20) Pineda, E. M.; Tuna, F.; Pritchard, R. G.; Regan, A. C.; Winpenny, R. E.; McInnes, E. J. Molecular Amino-Phosphonate Cobalt-Lanthanide Clusters. *Chem. Commun.* **2013**, *49*, 3522-3524.

(21) Pineda, E. M.; Tuna, F.; Zheng, Y.-Z.; Winpenny, R. E. P.; McInnes, E. J. Wells-Dawson Cages as Molecular Refrigerants. *Inorg. Chem.* **2013**, *52*, 13702-13707.

(22) Rajeshkumar, T.; Annadata, H. V.; Evangelisti, M.; Langley, S. K.; Chilton, N. F.; Murray, K. S.; Rajaraman, G. Acetic Acid-Assisted Solution Process for Growth of Complex Copper Sulfide Microtubes Constructed by Hexagonal Nanoflakes. *Inorg. Chem.* **2015**, *54*, 1661-1670.

(23) Gabrielle, D.; Rudolf A. HOW TO RECOGNIZE O^{2-}, OH^-, AND H_2O IN CRYSTAL STRUCTURES DETERMINED BY X-RAYS. *Am. Mineral*. **1970**, *55*, 1003-1015.

(24) Lun, H., Du, M., Wang, D., et al. Double-Propeller-like Heterometallic 3d-4f Clusters $Ln_{18}Co_7$. *Inorg. Chem.* **2020**, *59*, 7900-7904.